Laboratory study of linear and nonlinear elastic pulse propagation in sandstone

James A. Ten Cate, Koen E.A Van Den Abeele,[a)] Thomas J. Shankland, and Paul A. Johnson[b)]

Earth and Environmental Sciences Division, Mail Stop D443, Los Alamos National Laboratory, Los Alamos, New Mexico 87545

[a)] *also at K. U. Leuven Campus Kortrijk, Belgium, as Post-doctoral Fellow of the Belgian National Foundation for Scientific Research*
[b)] *also at Department de Recherches Physiques, Université Pierre et Marie Curie (Paris 6), Tour 22-4, Place Jussieu, 75252 Paris Cedex 05, France*

(Received:

We performed linear and nonlinear elastic wave pulse propagation experiments in sandstone rods, both at ambient conditions and in vacuum. The purpose of these experiments was to obtain a quantitative measure of the extremely large nonlinear response found in microcracked (*i.e.*, microinhomogeneous) media like rock. Two rods were used, (1) a 2 m long 5 cm diameter rod of Berea sandstone (with embedded detectors) used in previously published experiments and (2) a somewhat smaller 1.8 m long 3.8 cm diameter rod. In the earlier experiments, wave scattering from the embedded detectors was a critical problem. In most of the experiments reported here, this problem was avoided by mounting accelerometers directly to the outside surface of the smallest rod. Linear experimental results show out of vacuum attenuations varied from 1.7 Np/m at 15 kHz (Q=10) for the large rod to 0.4 Np/m at 15 kHz (Q=55) for the small rod; attenuations for the small rod in vacuum were much less, typically about 0.15 Np/m at 15 kHz (Q=150). Wave velocities ranged from 1900 m/s to 2600 m/s. The nonlinear results illustrate growth of the second and third harmonics and accompanying decay of the fundamental. These nonlinear results compare well with a numerical model. Although the results here were performed at peak strain amplitudes as low as 5×10^{-7}, they still show the pronounced nonlinearity characteristic of rock, in agreement with static and resonance studies using the same rock type.

PACS numbers: 43.25.Dc

INTRODUCTION

The micro-inhomogeneities characteristic of many rocks gives rise to some spectacular nonlinear elastic effects. In previous pulse-mode laboratory experiments, Meegan *et al.*[1] demonstrated that, under ambient conditions, harmonics of pure tone signals are generated along the wave propagation path in a Berea sandstone bar at strain levels as low as 3×10^{-6}. The experiments roughly confirmed predictions from perturbation theory[2] that the second harmonic amplitude grows linearly with propagation distance, with the square of the input frequency, and with the square of the fundamental amplitude. Resonance experiments conducted with the same rock type at similar strain levels also show pronounced effects associated with nonlinearity. The frequency at which Young's mode resonance occurs shifts noticeably with increasing drive amplitude for many types of rock, including Berea sandstone, and multiple harmonics are generated.[3] Static stress-strain measurements[4,5] using Berea sandstone samples show distinctly nonlinear stress-strain curves as well.

Model studies have been conducted with the solution of the progressive, 1-D nonlinear elastic equation of motion using an iterative Green function method where a perturbative solution was found to second order in the nonlinearity.[2,6] To compare with their experiments, however, Meegan *et al.* used the results only to first order in the nonlinearity and included visco-elastic, linear attenuation. Recent numerical simulations by Van Den Abeele[7] include nonlinearity to second order and agree with the experimental observations published by Meegan *et al.* However, the resonance and static stress-strain measurements noted in the previous paragraph suggest that a different model of the nonlinear elasticity inherent in rock samples may be more appropriate.[8] Hysteresis and end point memory appear to be important, even at the low strain levels of the pulse propagation experiments. Hence, this work was motivated by a desire to expand on the earlier experimental work and to provide additional observations in an effort to determine the limits of current analytical models of nonlinear wave propagation in rock.

I. THEORY

The classical theory of nonlinear wave propagation in elastic solids has been discussed and presented many times in the literature (see, for example, Refs. 9–11). To date, most of the theoretical work used to describe nonlinear propagation in micro-inhomogenous materials such as rock has followed along these lines. We have

compared calculations from a particular model (theoretical and numerical) developed by Van Den Abeele[6] with some of the experimental results presented in this paper.

The traditional approach of nonlinear elasticity begins with the equation of motion for propagation in an infinite elastic solid in the absence of dissipation written as

$$\rho \frac{\partial^2 u_i}{\partial t^2} = \frac{\partial \sigma_{ij}}{\partial x_j} \tag{1}$$

where ρ is the mass density, u_i is the displacement in the x_i direction (*not* the particle velocity), and σ_{ij} is the stress tensor. For 1-D motion in thin circular rods, the above equation simply becomes

$$\rho \frac{\partial^2 u}{\partial t^2} = \frac{\partial \sigma}{\partial x} \tag{2}$$

where the stress σ may be written in terms of the strain ϵ using a nonlinear version of Hooke's law as follows:

$$\sigma = E\epsilon \left[1 + \beta\epsilon + \delta\epsilon^2 + \cdots\right] \tag{3}$$

where E is Young's modulus and β and δ are higher order nonlinear coefficients. If a source function is present, it is usually added to the right hand side of Eq. (2). If we use Eq. (3) and the fact that the small signal elastic "bar" speed is $c_0 = \sqrt{E/\rho}$, Eq. (2) can be rewritten as

$$\frac{\partial^2 u}{\partial t^2} = c^2 \frac{\partial^2 u}{\partial x^2} \tag{4}$$

where

$$c^2 = c_0^2 \left[1 + 2\beta\epsilon + 3\delta\epsilon^2 + \cdots\right] \quad . \tag{5}$$

One of the original purposes of the experiments discussed in this paper was to approximate values of β and δ for the sandstone samples available to us.

We should point out that the traditional approaches of Thurston and Shapiro[12] and McCall[2] (which were adapted and modified by Van Den Abeele[6] and others) yield expressions for 1-D elastic wave propagation in an *infinite medium* and not a thin rod. Thus, although their stress-strain relation has the same form as Eq. (3), the constants are different. E, β, and δ in Eq. (3) replace combinations of the Lamé and Murnaghan coefficients, λ, μ and l, m, n, respectively. For example, for an infinite solid, $\mu(\lambda + 2\mu)/(\lambda + \mu)$ takes the place of E in Eq. (3). The resulting "bulk" wave speed c_0 is also different for an infinite solid—a well-known result. Thus, some care is required in comparing values for β and δ measured in a rod or an infinite solid.

Van Den Abeele's solution[6] is a higher order extension of the Green function perturbation technique used by McCall[2] particularly applied for a pulsed wave with arbitrary (discrete) Fourier spectrum. This technique was used to solve the wave equation for 1-D propagation in an infinite elastic medium. McCall's approach is especially useful as it allows the flexibility of prescribing any source function. Because the solution is a perturbation result, it is valid only for small distances from the source. To allow large propagation distances, Van Den Abeele adapted an iterative approach similar to Haran and Cook[13] by dividing the propagation path into several small sections and using the output spectrum from one section as the input source function for the next section. Moreover, linear attenuation can be added *ad hoc* at the end of each step in a manner similar to that used by Pestorius and Blackstock.[14]

II. EXPERIMENTAL ARRANGEMENT

The pulse propagation measurements reported here were made using two nearly homogeneous but anisotropic rods of Berea sandstone (Cleveland Quarries, Amherst, Ohio). The first rod is a 2 m long, 6 cm diameter rod used by Meegan *et al.* This bar has detectors (Valpey-Fisher pinducers, part VP-1093) epoxied inside the rod within small boreholes drilled at 45° angles at various points along the rod axis. The second rod is similar although somewhat shorter and smaller, 1.8 m long and 3.8 cm in diameter and not tapered at the end. In order to reduce scattering effects, we chose not to drill holes in this second rod. Instead of pinducers, several B&K 8309 accelerometers were mounted directly to the outside of the rock (using a cyanoacrylate glue and an activator), each oriented along the axial direction. Gluing the accelerometers onto the rod also allows flexibility in receiver spacing. A PZT-4A piezoelectric disk and tantalum inertial backload were epoxied onto the end of the rod as a source, as in the configuration used by Meegan *et al.* Because the opposite end of the rod was not tapered, care was taken so that pulses that propagated along the smaller bar were short enough that reflections from the far end never interfered.

The electronics attached to the source and receivers are depicted in Fig. 1. An Analogic 2020 arbitrary function generator was the signal source. It was programmed to repeatedly output a tone burst with a gaussian-shaped envelope. The output of the 2020 was fed into a Hafler Pro5000 audio amplifier connected to the piezoelectric disk via a transformer. The transformer was essential because the Hafler will not drive a purely capacitive load. Nonlinearity of the transformer was not a problem; measurements of the spectra of the electronic signals going into the source at all drive

levels showed that the harmonics of the drive frequency were all more than 55 dB below the fundamental. For both bars, the output of each detector was fed into a B&K 2635 Charge Amp and then on to a LeCroy 9420 Digitizing Oscilloscope or to an Analogic 652/6100B Waveform Analyzer. Signal-to-noise ratios were improved by repeating the tone burst several times and using standard linear averaging techniques. We should point out that Meegan *et al.* connected the output of each pinducer to a voltage preamplifier by way of a calibrated cable; we chose to use a charge amplifier and not worry about cable loading effects.[15]

The choice of source frequencies was limited by the length of the bar and by the possibility of exciting unwanted higher order modes. 1-D elastic wave propagation is easiest to treat theoretically so we attempted to excite only the lowest order longitudinal mode in the bar. Propagation speed of this lowest longitudinal mode (or Young's mode) is about 1900 m/s for the smaller sample—somewhat higher in vacuum—and about 2600 m/s for the larger rod. Thus, to obtain enough cycles to analyze before the arrival of the reflected pulse, we limited the lowest source frequency to about 10 kHz. Accelerometer bandwidth and the possibility of exciting higher order modes limited the highest source frequencies. Although the lowest order torsional mode propagates at any frequency (as well as a host of flexural modes), higher order modes do not propagate below their cutoff frequencies. These frequencies were calculated from the rod geometry and the bar and shear wave speeds for both rods.[16] We found that for the smaller rod, the next higher longitudinal and torsional modes can propagate if their frequencies are greater than about 35 kHz and 55 kHz, respectively. For the larger rod these frequencies are somewhat lower, 28 kHz and 44 kHz. In addition, there is one more limit to the highest source frequency: although the accelerometers have a mounted resonance frequency of 180 kHz, B&K specifications indicate their response is flat (magnitude and phase) only to 54 kHz. The B&K charge amplifiers connected to the accelerometers have a known flat *amplitude* response to 100 kHz and flat *phase* response to about 25 kHz. Beyond 25 kHz, the phase shifts upward very slowly, to nearly 30° at 100 kHz. Imperfect accelerometer mounting will lower all these frequencies. Thus, to obtain an accurate measurement of the harmonics and still avoid exciting higher order modes, source frequencies were kept below 20 kHz.

III. LINEAR MEASUREMENTS

Several measurements of linear elastic wave propagation in each of the sandstone bars were made. The purpose of these measurements was twofold. First, an extensive

comparison between theoretical elastic wave propagation in a sandstone rod and the actual, observed wave propagation has not been reported. Second, linear attenuation and wave speeds were required in model calculations. Most of these measurements were conducted with the small bar because Meegan *et al.* had already conducted many linear measurements in the larger bar.

During the initial measurements with the small rod, we (re)discovered something known to Rayleigh, "The difficulty of exciting purely longitudinal vibrations in a bar is similar to that of getting a string to vibrate in one plane."[17] As already noted, the source frequencies used for these experiments permit propagation of both the lowest order longitudinal and torsional modes as well as a host of flexural modes. Although flexural modes are possible, they typically propagate with very slow speeds, are dispersive, and thus can be distinguished from other modes. Although our source condition does not favor torsional mode excitation, we nevertheless found that certain source frequencies do, in fact, readily excite a strong mode that propagates at the torsional (shear) velocity and exhibits a twisting motion associated with the lowest order torsional mode (see [18] for similar experimental results).

Figure 2 shows examples of tone bursts recorded in both the small, (a) and (c), and large (b) bar. Figure 2(a) shows a 1 ms long tone burst detected 85 cm from the source. Compare this waveform with Fig. 2(b), a tone burst detected in the larger bar 38 cm from the source. The tone burst in the larger bar is much cleaner, perhaps because the detectors were not mounted on the surface but located near the center of the rod where torsional motion does not (theoretically) exist. A shorter tone burst (0.3 ms long) detected at 60 cm in the smaller bar, Fig. 2(c), illustrates an arrival which is apparently the lowest torsional mode. The wave traveled with the shear wave velocity, was nondispersive, and, when another accelerometer was surface-mounted perpendicular to the original orientation, exhibited a strong twisting motion characteristic of the torsional mode. We attempted to avoid frequencies that generated torsional modes for all the experiments reported here.

The accelerometer orientation also posed some interesting measurement problems. Each accelerometer has a transverse sensitivity that is usually negligible. However, near the transverse resonance frequency and with the proper orientation, the measured transverse acceleration can be fairly large. For the B&K 8309s, the transverse sensitivity is a maximum at 28 kHz, very near the second harmonic in many of our experiments. We tried mounting the accelerometers with orientations in two different ways, to maximize or minimize the transverse response. The purpose of the

first orientation was to see how much torsional mode (twisting motion) was present; the purpose of the second orientation was to decouple the torsional mode from the longitudinal mode signal. As noted above, problems with unwanted torsional modes affecting the received signals are minimal with the detectors imbedded in the larger bar.

Measurements of both wave speed and attenuation are illustrated in the next group of figures. Figure 3 shows a typical range stack from several accelerometers mounted on the small bar. Note the clean waveforms at this frequency; torsional or flexural modes are not evident. As the figure shows, it is easy to follow a particular piece of the tone burst waveform and determine wave speed from the slope. The wave speed for the larger bar agrees well with the value of Meegan *et al.* (2700 m/s). We should also note that wave speeds did vary somewhat from day to day depending on ambient temperature, pressure, and humidity. The in-vacuum measurements, on the other hand, varied much less. Wave speeds for the smaller bar were 1950 m/s and 2100 m/s out and in vacuum, respectively.

An attenuation measurement for the smaller bar was not straightforward. The simplest technique—plotting the wave amplitude as a function of distance—did not work because site effects at each detector make determination of the decay uncertain. (Site effects are discussed in the Appendix.) Instead, we used a 0.5 ms long tone burst and recorded the original toneburst and five of its successive reflections from both ends of the rod. This was done at three separate accelerometer positions. Results for the small rod *in vacuum* are plotted in Fig. 4. Because a single accelerometer is used for each of the three data sets shown, site response is irrelevant. The average value of the attenuation α for the small bar in vacuum at 15 kHz was 0.16 Np/m ($\pm$ 0.02 Np/m). The equivalent average value for $Q_E = \pi f/(\alpha v)$—where Q_E is the extensional quality factor and v is the velocity of the Young's mode[19]—is 143 ($\pm$ 10). The solid vertical lines in the figure represent places where the tone burst is reflected from the source end. Data points taken after that reflection are expected to have additional energy loss because the reflected and incident pulse overlap and the exact nature of the reflection at the source end is not known. Indeed, the value of the attenuation taking the average value of the slope of only the first two data points is somewhat smaller, 0.13 Np/m ($Q_E \approx 180$). A similar experiment done at the same frequency with the rod *out* of vacuum yielded an attenuation of 0.4 Np/m ($Q_E = 55$). For the larger bar the attenuation out of vacuum has been measured to be much higher due to wave scattering from the imbedded pinducers; Meegan *et al.*

report a Q=10 which corresponds to $\alpha = 1.7$ Np/m at 15 kHz.

The linear experiments also revealed that the lowest longitudinal mode does not develop immediately after it is emitted by the source. Several B&K 4374 accelerometers were mounted within 20 cm of the source oriented to measure the radial acceleration along the rod since Young's mode is frequently described as a "snake swallowing" motion. Figure 5 shows the results. It is apparent that there is much less radial motion near the source than farther down the rod. Generally, we found that it was not until the wave had propagated a distance of about one to two wavelengths that the axial and concommitant radial motions that characterize Young's mode were present. Therefore, all measurements on the small rod were made at a distance greater than 20 cm from the source where a fully developed Young's mode *was* evident. To our knowledge, the development of Young's mode shown here has not been discussed elsewhere in the literature.

IV. NONLINEAR MEASUREMENTS

As a starting point we repeated some of the experiments conducted by Meegan *et al.* We chose to use a B&K 8309 accelerometer glued to the backload instead of the optical probe previously used; the accelerometers are far less noisy and are more sensitive in general. We assumed thoughout these experiments that the accelerometer gave an accurate representation of the *relative* spectrum of the source acceleration. Absolute source spectrum values, where required, were estimated. Figure 6 shows a typical source spectrum obtained at the backload for a high source strain level. It is rich in harmonics. Because Meegan *et al.* had an exceptionally clean source signal (see their Fig 3),[1] we presume that the bond between transducer and rock had degraded since the earlier work. Such a rich source spectrum had an unexpected effect on the results; harmonics at the source tended to mask whatever nonlinear effects we might have seen. In fact, the presence of source harmonics changed the experimental results dramatically (which will be discussed subsequently).

If the spectrum at the backload is taken as the source function for Van Den Abeele's[7] numerical method and β, δ, and Q_E are chosen to be 500, 1×10^7, and 10, respectively, we can make the comparison shown in Fig. 7. Predicted theoretical spectral levels at each harmonic are indicated with circles, and the measured spectra are shown as solid lines. Two things should be noted. As we commented earlier, source harmonics masked nonlinear effects, i.e., the values of β and δ chosen above were small enough that they had no effect on the model calculations.[20] Second, measured peak values

at the various harmonics seen in the figure fluctuate around the predicted level. This behavior illustrates the problem of *site response*. Our solution to the site response problem is discussed in detail in the Appendix.

Rather than repeating more experiments on the large bar or remounting the source, we performed additional experiments on a somewhat smaller sample. The same source configuration was used on the small bar as on the larger bar. Unfortunately, we were unable to produce a clean, relatively monotonal source pulse like that shown by Meegan *et al.* However, certain source frequencies proved to be better choices than others. Figure 8 shows a typical spectrum from a 12.4 kHz source obtained from a B&K 4374 accelerometer mounted on the Ta backload with the bar in air. It should be noted that the resonance frequency of the B&K 4374 accelerometer is somewhat lower than the accelerometers normally used (B&K 8309) so the upper frequency end of the spectrum—from about 40 kHz on—is somewhat enhanced. However, we were interested only in the behavior of the 2nd and 3rd harmonics, which were safely in the lower end of the spectrum. Maximum source levels were estimated to be about 10 dB lower than the maximum levels reported by Meegan *et al.*; peak strain amplitudes are about 5×10^{-7}. The second harmonic shown in this figure is about 10 dB lower than the fundamental; on the other hand, the 3rd harmonic at 37.2 kHz is much lower and is, in fact, hard to identify. The peak at 40 kHz (which is not a multiple of the source frequency) may be due to resonance of the PZT disk which has a designed center frequency of 40 kHz. Spectra taken at the backload in vacuum were similar although 2nd and 3rd harmonic levels were usually higher than the out-of-vacuum spectra.

Spectral ratios as a function of distance at various source frequencies were obtained with the small rod in vacuum. In all cases, backload source spectra indicated a distorted source and were similar to the spectrum shown in Fig. 8. Figures 9(a) and (b) show plots of fundamental, second, and third harmonic spectral ratios (denoted R1, R2, and R3.) *versus* distance for drive frequencies of 13 kHz and 14 kHz, respectively. In both cases the 2nd harmonic at the source was only about 5 dB lower than the fundamental. The 3rd harmonic at the source, however, was very low and, in fact, hard to identify at 13 kHz (39 kHz). Both figures show a second harmonic that does not grow or grows just slightly (b). This is not an unexpected result considering the large 2nd harmonic in the source spectrum.[6] Both figures do, however, show strong 3rd harmonic growth with distance. For completeness, the spectral ratios for the fundamental are also shown in both plots; in both cases the lines are nearly flat.

This behavior also is expected based on simulations. Other in-vacuum results are similar to those shown here.

Finally, we made measurements of the spectral ratios as a function of distance for the 2nd and 3rd harmonics *out* of vacuum. Source spectra were typically cleaner than those taken with the bar in vacuum. Fig. 10(a) shows a plot of spectral ratios obtained with the source spectrum shown in Fig. 8. Spectral ratios for the second and third harmonic are denoted R2 and R3. The two lines (least squares fits) are shown to guide the eye and do not necessarily represent the true functional dependence of spectral ratio on distance. The errors in the method and sparseness of data do not allow us to deduce the exact functional forms. However, the error bars *are* significantly smaller than the spread in each case and both harmonics are growing with distance. Fig. 10(b) shows a simulation of the experiment using the numerical model with values of β, δ, and Q_E of 400, 2×10^8, and 55, respectively. The results are very similar, especially considering the uncertainties in (1) determining the true source function and (2) exciting pure small signal waves at the second and third harmonic frequencies and determining source levels. Although we believe other nonlinear effects must be accounted for in the model, these results clearly show that the nonlinearity inherent in rocks manifests itself at levels even lower than initially reported by Meegan *et al.*

V. SUMMARY AND CONCLUSIONS

The results of several experiments examining linear and nonlinear wave propagation in two Berea sandstone rods have been reported and compared with a numerical model. Small amplitude wave speeds were measured in both samples, both in and out of vacuum and found to range from 2600 m/s to 1900 m/s. Small signal attenuation was also measured and varied considerably, depending on whether the sandstone bar was inside or out of vacuum. Values of Q_E ranged from 10 (large sample in air) to 150 (small sample in vacuum). Measurements were made of higher strain amplitude waves too. Nonlinearity is clearly evident in our measurements. Most of the new measurements were obtained using a smaller, thinner rod than the study by Meegan *et al.*[1] and, since the detectors were surface mounted, wave scattering was not a problem. Remarkably, propagation of waves with peak strain levels of only 5×10^{-7} clearly show the effects of nonlinearity (10 dB lower than levels used in Meegan *et al.*). The results also clearly show both 2nd *and* 3rd harmonic growth. A numerical algorithm[6] which includes second order nonlinear constants in the equation of state was used to compare with the data presented here and the results are very good. The data

presented here nicely complement and greatly add to the data presented by Meegan *et al.*

Comparison of measurements and calculations, however, strongly suggest that the current theory is incomplete.[7] Moreover, considerable evidence from resonance and static stress-strain studies on similar materials suggests that hysteresis and end point memory[3,5] likely play prominent roles in wave propagation in earth materials such as rock. Some preliminary numerical work by Van Den Abeele[23] is promising. He has added hysteresis in his model and has shown that harmonics at levels we have observed in these measurements can easily be generated without requiring large δ's. Work is continuing along these lines.

ACKNOWLEDGMENTS

This work was supported by the Office of Basic Energy Sciences-Geosciences of the Department of Energy through the University of California. We also wish to thank Doug Meegan, Robert Guyer, and Katherine McCall for valuable discussions and suggestions.

APPENDIX. SITE RESPONSE AND SPECTRAL RATIOS

Measurements with earth materials are typically much more difficult than those conducted in air or water. Site response, the variation in signal intensity due to local inhomogeneity and detector coupling, is a well-known problem in seismology, and laboratory experiments on solids share some of the same difficulties. In seismology, the observed spectrum at a ground location is often expressed as the true source spectrum (at depth) passed through a series of linear filters. Filters that are often used include instrument response, propagation path response, geometric spreading, source radiation response, etc.[22] In our 1-D rod experiments we need only correct for source, instrument, and path response (including attenuation, nonlinear response, etc...). Attenuation along the propagation path is relatively easy to determine. However, accelerometer site response is not. Ideally, if the mounting is perfect, the B&K accelerometers have a flat response to 54 kHz. However, a perfect mounting is rarely possible, especially on porous sandstone rods. Imperfect mounting will lower the resonance frequency and alter the expected accelerometer frequency response. Moreover, the rod itself is anisotropic and not perfectly homogenous so different mounting

points will yield slightly different accelerations. The problem is even more troublesome with the pinducers as they are not calibrated.[21] Figure 7 shows the effects of site response; variations of the spectra from site to site are obvious at any frequency.

A widely applied method used for eliminating site response in seismology is the method of spectral ratios. In earthquake studies for example, the effects of wave travel paths, attenuation, and seismometer variations can be cancelled by taking the ratio of a large earthquake spectrum to a much smaller earthquake spectrum from the same source location.[22] We have adapted the technique to eliminate the site response problem in our laboratory experiments as follows. Assume for simplicity that we have a source whose spectrum consists of a single line at frequency f_1, i.e., a monotonal source. The measured small-strain spectral level for this line $M(f_1, x_i)$ from an accelerometer at a distance x_i from the source can be represented as the source spectrum $S(f_1)$ passed through two linear filters:

$$M(f_1, x_i) = A(f_1, x_i) \cdot \Psi(f_1, x_i) \cdot S(f_1) \tag{A1}$$

where $A(f_1, x_i)$ is the filter representing the attenuation evaluated at f_1 and $\Psi(f_1, x_i)$ is the filter representing the detector site response evaluated at f_1. If we supply a second monotonal source spectrum S'—at the same frequency but at a different small-strain amplitude—the same filters apply and the ratio of the two measured spectral lines is simply

$$R(f_1) = \frac{M'(f_1, x_i)}{M(f_1, x_i)} = \frac{S'(f_1)}{S(f_1)} \quad . \tag{A2}$$

In this case (two linear source functions), R is a constant for all positions x_i.

Application of the spectral ratio method to a large amplitude (i.e., *nonlinear*) and small elastic wave signal requires some modification. We therefore use a hybrid approach. Assume we excite a large amplitude single source frequency $S_N(f_1)$ and measure the resulting nonlinear wave spectrum (rich in harmonics) $M(nf_1, x_i)|_{n=1,2,3,\cdots}$ at a distance x_i from the source. Instead of exciting only a low amplitude wave at f_1, we also separately excite and measure small amplitude waves at $2f_1$, $3f_1$, etc. We then take the ratio of the appropriate spectral line in the nonlinear signal to each of the small amplitude harmonics. The measured levels for each of the *low amplitude* signals, given the source functions $S(nf_1)$ are

$$M(nf_1, x_i) = A(nf_1, x_i) \cdot \Psi(nf_1, x_i) \cdot S(nf_1) \qquad n = 1, 2, 3, \cdots \tag{A3}$$

and the measured levels in the *nonlinear* spectrum given the source function $S_N(f_1)$ are

$$M_N(nf_1, x_i) = A_N(nf_1, x_i) \cdot \Psi(nf_1, x_i) \cdot S_N(f_1) \qquad . \tag{A4}$$

Note that we assume site response Ψ is independent of amplitude. The ratio of the measured large amplitude signal driven at f_1 at the nth harmonic to the low amplitude signal driven at nf_1 is

$$R_n = \frac{M_N(nf_1, x_i)}{M(nf_1, x_i)} = \frac{A_N(nf_1, x_i)}{A(nf_1, x_i)} \left[\frac{S_N(f_1)}{S(nf_1)}\right] \tag{A5}$$

The site response Ψ is again eliminated and the source ratio is a constant. The new attenuation "filter" response A_N now contains the nonlinear propagation effects (e.g., decay of the fundamental or growth of a harmonic). For the harmonics above the fundamental, for example, the ratio $A_{NL}(nf_1, x_i)/A(nf_1, x_i)$ should increase with distance if the rod responds nonlinearly. This method appears to work very well in the case of a source that does not emit harmonics. Indeed, Meegan *et al.* successfully applied this formulation to plot the ratio R_2 as a function of distance. If nonlinearity in the material had not been present, the ratio would have been constant for all pinducer positions. What Meegan *et al.* found, however, was that the value of the spectral ratio appeared to grow linearly with x, exactly what classical theory predicted, a convincing show of nonlinear response in the material.

A cautionary note: if the source emits harmonics, problems are introduced into the method. A rich source spectrum translates to a redistribution of energy within the wave spectrum along the path in a complex manner because interactions between all frequencies begins immediately. See Van Den Abeele[6] for more discussion on contaminated sources and their effects on the simple harmonic relationships.

REFERENCES

[1]G.D. Meegan, Jr., P.A. Johnson, R.A. Guyer, and K.R. McCall, "Observations of nonlinear elastic wave behavior in sandstone," *J. Acoust. Soc. Am.* **86**, 2309–2317 (1989).

[2]K.R. McCall, "Theoretical study of nonlinear elastic wave propagation," *J. Geoph. Res.* **99**, 2591–2600 (1994).

[3]P.A. Johnson and P.N.J. Rasolofosaon, "Manifestation of nonlinear elasticity in rock: Convincing evidence over large frequency and strain intervals from laboratory studies," *Nonlinear Geophysics*, 1995 (in review).

[4]L.B. Hilbert, Jr., T.K. Hwong, N.G.W. Cook, K.T. Nihei, and L.R. Myer, "Effects of strain amplitude on the static and dynamic nonlinear deformation of Berea sandstone," *Rock Mechanics Models and Measurements: Challenges from Industry*, P.P. Nelson and S.E. Laubach, eds., (A.A. Balkema, Rotterdam, 1994) 497–504.

[5]R.A. Guyer, K.R. McCall, and G.N. Boitnott, "Hysteresis, discrete memory and nonlinear wave propagation in rock," *Phys. Rev. Lett.*, **74**, 3491–3494 (1995).

[6]Koen E-A Van Den Abeele, "Elastic pulsed wave propagation in media with second or higher order nonlinearity. Part I: Theoretical framework" submitted to *J. Acoust. Soc. Am.*, May 1995.

[7]Koen E-A Van Den Abeele, "Elastic pulsed wave propagation in media with second or higher order nonlinearity. Part II: Simulation of experimental measurements on Berea sandstone" submitted to *J. Acoust. Soc. Am.*, May 1995.

[8]K.R. McCall and R.A. Guyer, "Equation of state and wave propagation in hysteretic nonlinear elastic materials," *J. Geoph. Res.* **99**, 23887–23897 (1994).

[9]L.D. Landau and E.M. Lifshitz, *Theory of Elasticity*, 3rd ed., (Pergamon, New York, 1959).

[10]F.D. Murnaghan, *Finite Deformation of an Elastic Solid*, (John Wiley & Sons, New York, 1951).

[11]A.L. Polyakova, "Nonlinear effects in a solid," *Sov. Phys. Solid State*, **6**, 50-54 (1964).

[12]R.N. Thurston and M.J. Shapiro, "Interpretation of ultrasonic experiments on finite-amplitude waves," *J. Acoust. Soc. Am.* **41**, 1112–1125 (1967).

[13]M.E. Haran and B.D. Cook, "Distortion of finite amplitude ultrasound in lossy media," *J. Acoust. Soc. Am.* **73**, 774–779 (1983).

[14]F.M. Pestorius and D.T. Blackstock, "Propagation of finite-amplitude noise," *Finite-Amplitude Wave Effects in Fluids*, Proceedings of the 1973 Symposium, Copenhagen, Denmark, ed. L. Bjørno, (IPC Science and Technology Press, Surrey, England, 1974).

[15]M. Serridge and T.R. Licht, *Piezoelectric Accelerometers and Vibration Preamplifiers. Theory and Application Handbook*, (Brüel & Kjær, Glostrup, Denmark, 1987).

[16]K.F. Graff, *Wave Motion in Elastic Solids*, (Ohio State University Press, 1975).

[17]J.W.S. Rayleigh, *The Theory of Sound*, (Dover Publications, New York, 1945), pp. 242-243.

[18]H. Kwun and C.M. Teller, "Magnetostrictive generation and detection of longitudinal, torsional, and flexural waves in a steel rod," *J. Acoust. Soc. Am.* **96**, 1202–1204 (1994).

[19]Society of Exploration Geophysicists, *Seismic Wave Attenuation*, Geophysics reprint series No. 2, D.H. Johnston and M.N. Toksöz, eds., pp. 1–5, (1981).

[20]The initial values of β and δ were chosen from work present by Van Den Abeele in Ref. [6].

[21]The pinducers are furnished uncalibrated. For these frequencies, they appear to have a fairly flat acceleration response with frequency. To get displacement spectra, each epoxied pinducer would have to be calibrated for the frequencies of interest with a known displacement detector. The only displacement detector available to us was the optical probe which was very noisy.

[22]W.H. Bakun and C.G. Bufe, "Shear-wave attenuation along the San Andreas fault zone in central California," *Bull. Seism. Soc. Am.* **65**, 439–459 (1975).

[23]Koen Van Den Abeele, personal communication.

Figure Captions

1. Experimental Setup: Block diagram shows source drivers and one detector channel.

2. Typical received tone bursts. Top waveform (a) was obtained from an accelerometer on the surface of the small bar, 85 cm from the source with a source frequency of 15 kHz and a 1 ms long tone burst. Middle waveform (b) was obtained from a pinducer in the large bar, 38 cm from the source with a source frequency of 14 kHz and a 1 ms tone burst. Bottom waveform (c) was obtained from an accelerometer on the surface of the small bar, 60 cm from the source with a source frequency 19 kHz and a 0.3 ms tone burst. Time axes of the top two plots have been shifted in order to show all tone bursts on the same scale.

3. Typical rangestack used to calculate pulse propagation speed. Data taken from accelerometers on small bar, under vacuum ($\leq$20 mTorr) with 0.5 ms tone bursts at 15 kHz source frequency. Each waveform amplitude has been normalized. Dashed line tracks the first arrival of the tone burst and the dot-dashed line tracks its reflection from the far end of the bar.

4. Peak acceleration values for an initial tone burst and its five later (multiple reflection) arrivals. Squares represent data taken at an accelerometer 28 cm from the source, circles 35 cm from the source, and diamonds 50 cm from the source. Solid, dotted, and dash-dotted lines represent least squares fits to each position, respectively. Vertical lines at 3.6 m and 7.2 m represent points where the tone burst is reflected from the source end.

5. Output of several accelerometers (oriented to be sensitive to radial r motion) mounted near the source operating at 12 kHz on the small bar. Different symbols indicate different runs.

6. Spectrum (magnitude) of a large amplitude source signal taken from a B&K 8309 accelerometer mounted on the rear face of the Ta backload. Driving frequency was 13.75 kHz.

7. Model calculations (circles) and measured acceleration spectra (solid lines) for an intense tone burst travelling down the large sandstone rod. Order of spectra

is left to right, the upper left hand corner corresponding to the spectrum taken 2.5 cm from the source. Pinducers are separated by 5 cm thereafter.

8. Source spectrum taken at the source backload of the small bar in air with a B&K 4374 accelerometer. Driving frequency was 12.4 kHz.

9. Spectral ratios as a function of propagation distance for fundamental (circles), 2nd (squares), and 3rd (triangles) harmonics. Source frequencies were (a) 12 kHz and (b) 13 kHz, and source strain amplitude estimated at 3×10^7. All data were taken with the rod in a vacuum of at least 10 mTorr.

10. (a) Spectral ratios as a function of propagation distance for 2nd (squares) and 3rd (triangles) harmonics. Source frequency was 12.4 kHz, source strain amplitude estimated at 2×10^7. Bar was in air. Lines are least squares fits to guide the eye. (b) Calculated spectral ratios for values of β, δ, and Q_E of 400, 2×10^8, and 55, respectively.

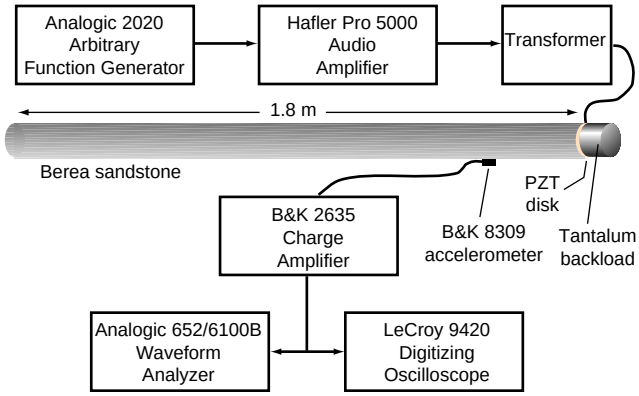
Analogic 2020
Arbitrary
Function Generator
Hafler Pro 5000
Audio
Amplifier
Transformer
1.8 m
Berea sandstone
PZT
disk
B&K 2635
Charge
Amplifier
B&K 8309
accelerometer
Tantalum
backload
Analogic 652/6100B
Waveform
Analyzer
LeCroy 9420
Digitizing
Oscilloscope

Fig. 1

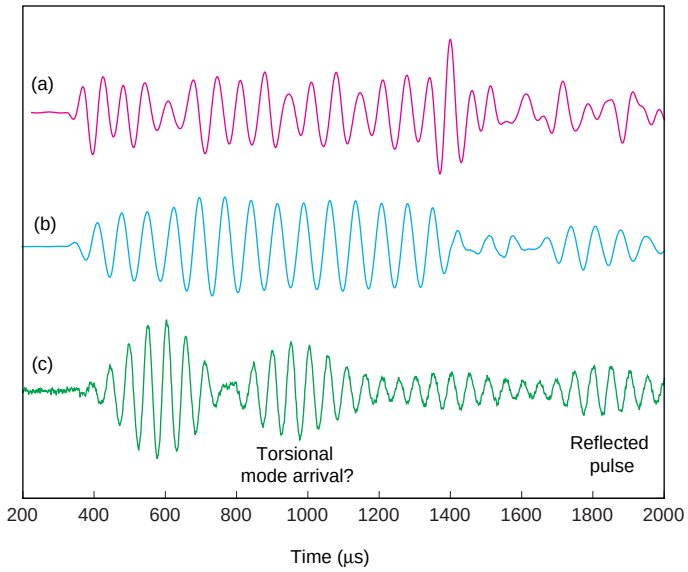
(a)
(b)
(c)
Torsional
mode arrival?
Reflected
pulse
200
400
600
800
1000
1200
1400
1600
1800
2000
Time (μs)

Fig. 2

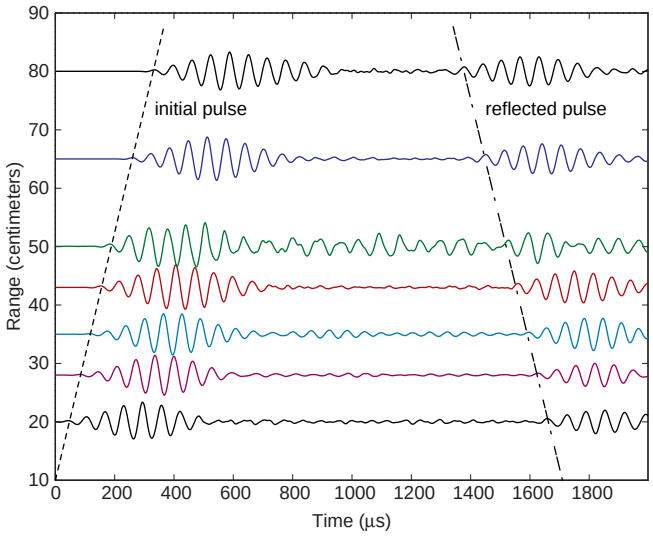
initial pulse
reflected pulse
Range (centimeters)
Time (μs)
90
80
70
60
50
40
30
20
10
0
200
400
600
800
1000
1200
1400
1600
1800

Fig. 3

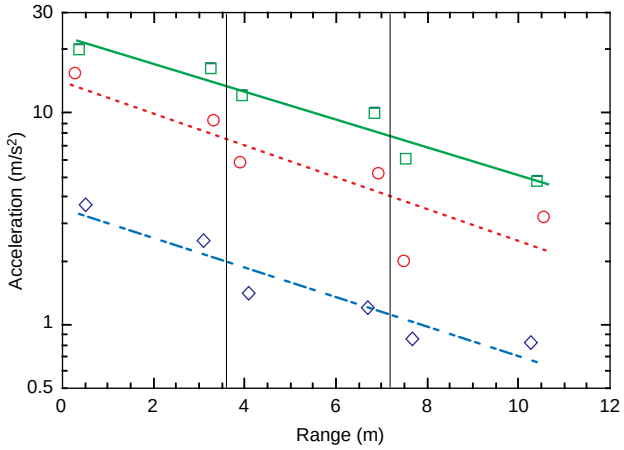

Fig. 4

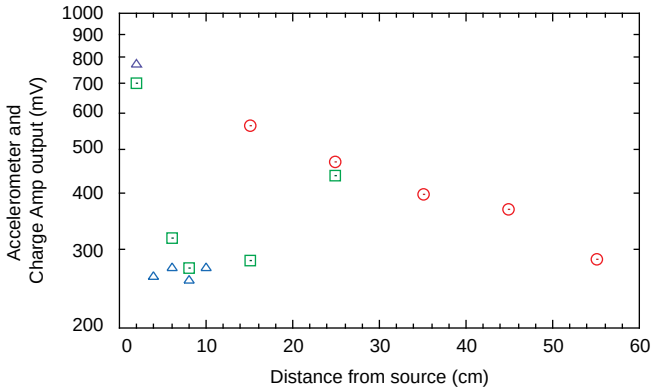
Accelerometer and
Charge Amp output (mV)
1000
900
800
700
600
500
400
300
200
0
10
20
30
40
50
60
Distance from source (cm)

Fig. 5

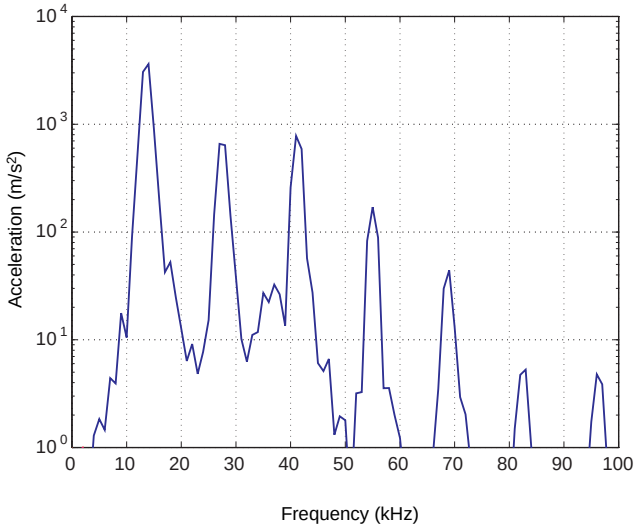
10^4
10^3
10^2
10^1
10^0
Acceleration (m/s^2)
0
10
20
30
40
50
60
70
80
90
100
Frequency (kHz)

Fig. 6

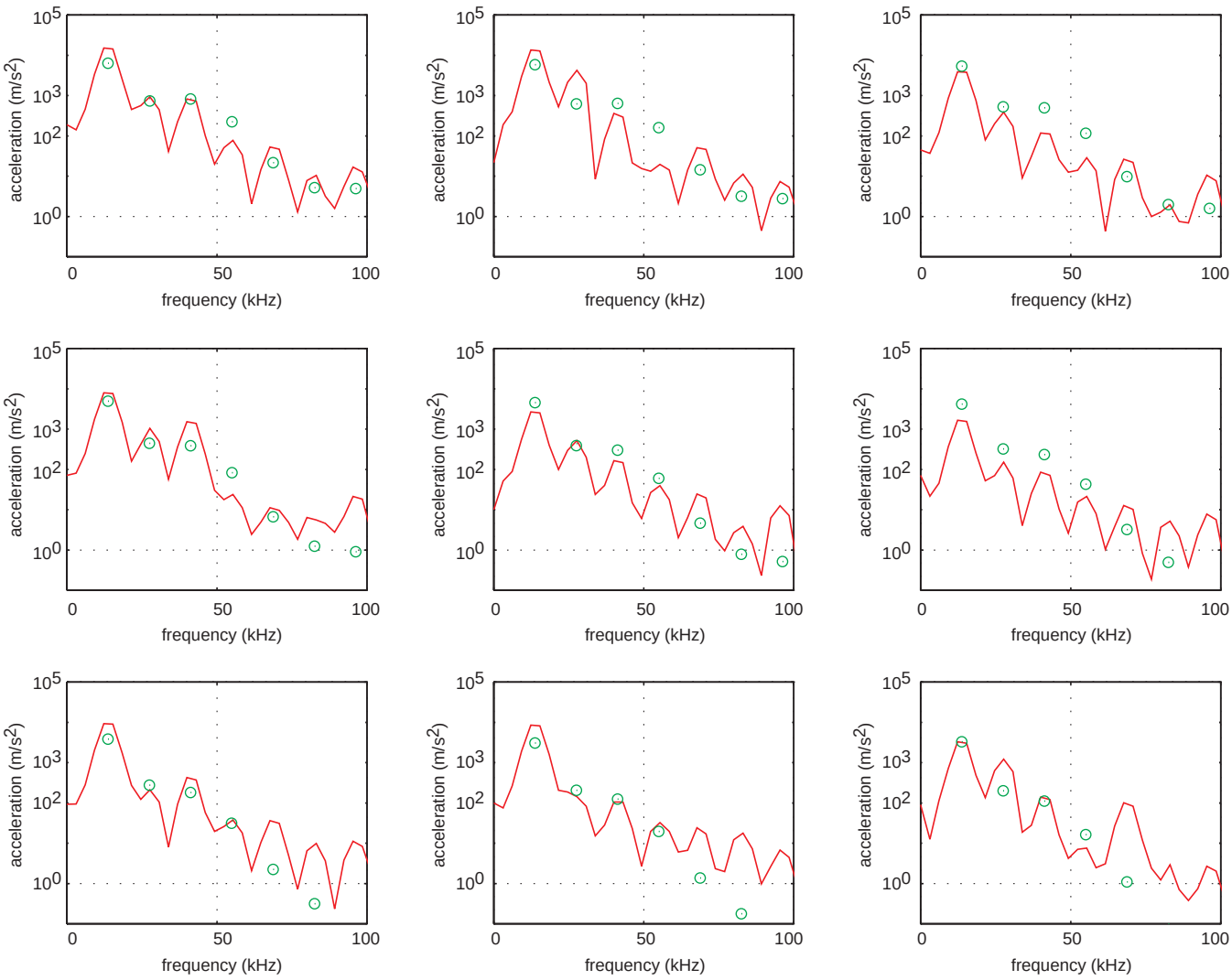

Fig. 7

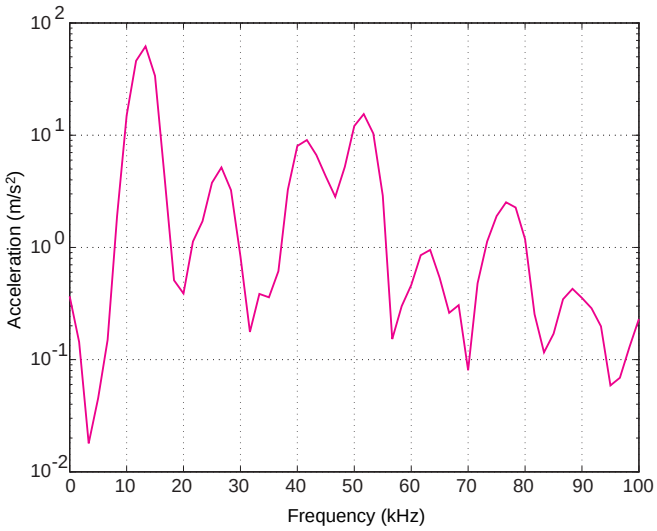
10^2
10^1
10^0
10^-1
10^-2
Acceleration (m/s²)
0
10
20
30
40
50
60
70
80
90
100
Frequency (kHz)

Fig. 9

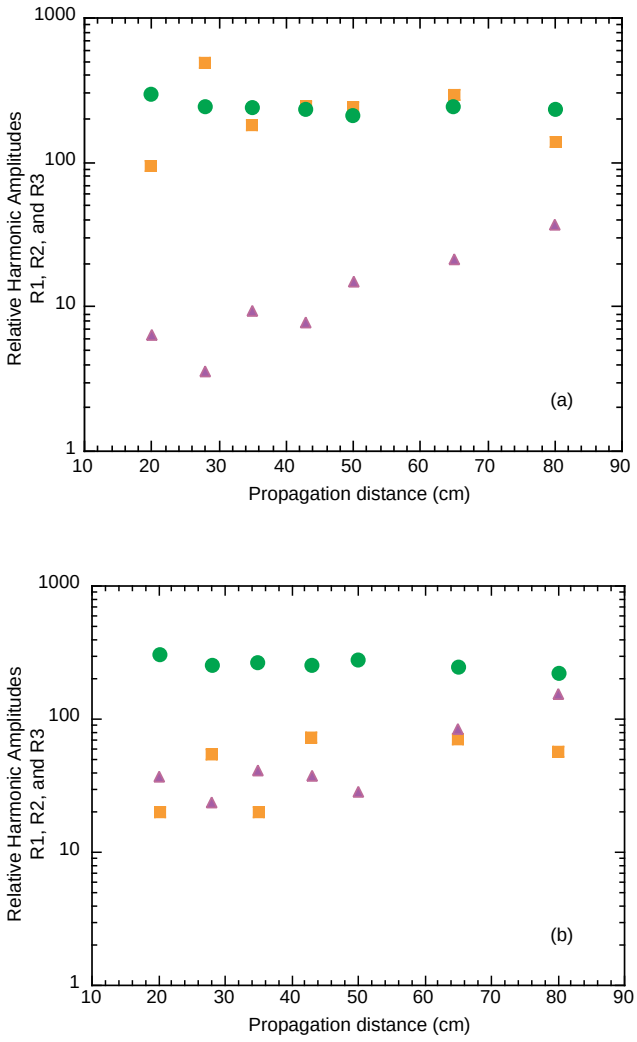
1000
100
10
1
Relative Harmonic Amplitudes
R1, R2, and R3
(a)
10
20
30
40
50
60
70
80
90
Propagation distance (cm)
1000
100
10
1
Relative Harmonic Amplitudes
R1, R2, and R3
(b)
10
20
30
40
50
60
70
80
90
Propagation distance (cm)

Fig. 10

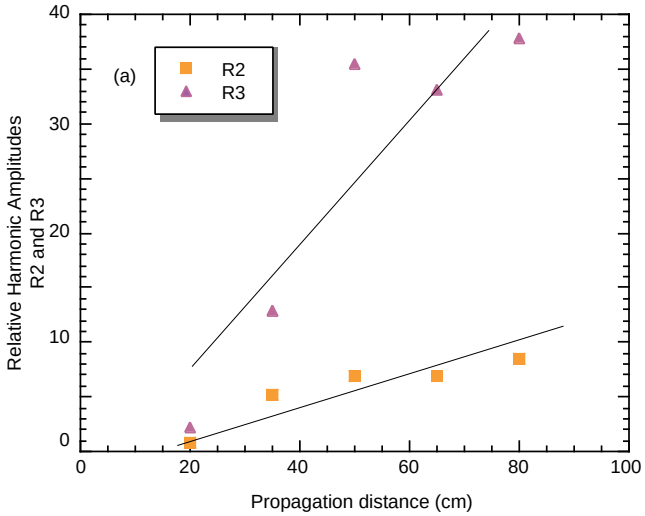
(a)
R2
R3
Relative Harmonic Amplitudes
R2 and R3
Propagation distance (cm)
0
10
20
30
40
0
20
40
60
80
100

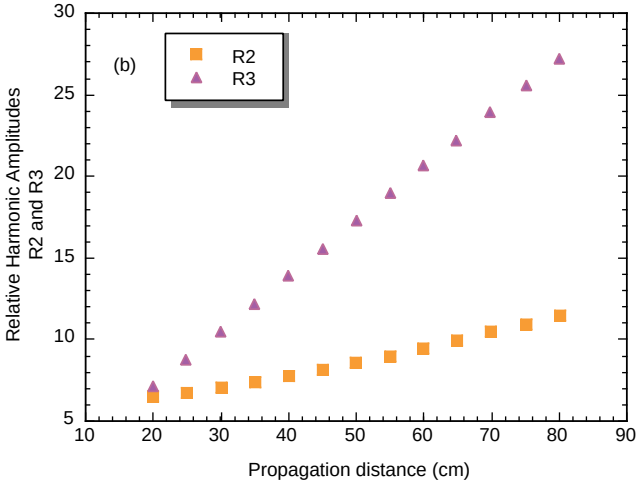
(b)
R2
R3
Relative Harmonic Amplitudes
R2 and R3
Propagation distance (cm)
5
10
15
20
25
30
10
20
30
40
50
60
70
80
90

Fig. 11